Environmental Science and Pollution Research (2021) 28:56782–56794
https://doi.org/10.1007/s11356-021-14662-3

RESEARCH ARTICLE

Sorption of Ce(III) on magnetic/olive pomace nanocomposite: isotherm, kinetic and thermodynamic studies

Yusuf Azmi Akbas[1] · Sabriye Yusan[1] · Senol Sert[1] · Sule Aytas[1]

Received: 20 January 2021 / Accepted: 27 May 2021 / Published online: 1 June 2021

Abstract
Used for various high-tech applications, cerium is an important rare earth element (REE), and its sorption on various solids also is important considering purification and environmental and radioactive waste disposal. In view of the industrial and environmental terms, it is important to remove Ce^{3+} ions from an aqueous solution. Magnetite and magnetic olive pomace nanocomposite were thus fabricated by a partial reduction co-precipitation approach. The structure and morphological properties of the prepared nanomaterial and nanocomposite were characterized by means of scanning electron microscopy (SEM), transmission electron microscopy (TEM), X-Ray diffraction (XRD), Fourier transform infrared spectrometry (FT-IR), vibrating sample magnetometry (VSM), and BET surface area analysis. The effects of parameters such as solution pH, contact time, initial Ce(III) concentration, and temperature on the sorption efficiency were studied. The maximum sorption capacities of the magnetite (MNP) and magnetic olive pomace nanocomposite (MOP) for Ce(III) ions were found to be 76.92 and 90.90 mgg^{-1}, respectively. The sorption data fitted well with Dubinin-Radushkevich isotherm model and the pseudo-second-order kinetic model. Thermodynamic parameters indicated that the sorption was non-spontaneous and endothermic. This paper reports the preparation of MNP and novel MOP and their application as efficient, sustainable adsorbents alternative to commercial ones for adsorption of cerium ions from aqueous solution.

Keywords Olive pomace · Magnetite · Nanocomposite · Cerium · Sorption

Introduction

Cerium is the first discovered and the most abundant element of the group of rare earth elements. As well as in combination with other rare earth elements, it is found in the spent nuclear fuel (Dubey and Rao 2011). Cerium accumulates in soil and sediments, and its concentration in humans, animals, and soils is on the increase (Ramos et al. 2016). It affects cell membranes in aquatic animals and has an adverse effect on reproduction and nervous systems (Loddo et al. 2020). Cerium can also be dangerous for humans (Rim et al. (2013). Likely to be encountered in domestic products such as television screens and fluorescent lamps, it causes pulmonary embolism in case of prolonged exposure (Nemmar et al. 2017). The accumulation in human body also endangers the liver (Dubey and Rao 2011).

Therefore the effective and economical process to remove rare earth ions from aqueous solution has attracted widespread attention. Sorption method is a good choice to remove rare earths elements from aqueous solutions due to its advantages such as popularity, low cost, easy operation, and convenience. Many studies have addressed the application of agro-wastes sorbents to the sorption of precious metals from aqueous solutions or to the recovery of heavy metals from waste streams (Kutahyali et al. 2012; Akbas and Yusan 2020; Torab-Mostaedi 2013).

The waste of the olive oil production process is called the olive pomace, which is obtained in abundance in the Mediterranean countries in particular thanks to large-scale production of olive oil (Aljerf and Choukaife 2015). Its high amount makes it important to reuse itself. Olive pomace is made up of almost all the structural lignocelluloses, as economic and environment friendly biosorbent (Toro 2003). Its organic structure contains 37.06% cellulose, 29.39%

Responsible Editor: Angeles Blanco

✉ Sabriye Yusan
sabriyeyusan@gmail.com

[1] Ege University Institute of Nuclear Sciences, 35100 Bornova, Izmir, Turkey

hemicellulose, and 33.65% lignin, which is not harmful to the environment, with a high surface area. Therefore, olive pomace has been the subject of many studies (Doyurum and Celik 2006). The most commonly known compound of the iron oxide is Fe_3O_4, which is the most magnetic mineral in the world. Accordingly, it is termed magnetite. Fe_3O_4 nanoparticles are caused by precipitation of iron salts in the alkaline environment (Ajinkya et al. 2020). Nano magnetite mineral has usage in the environmental studies, biomedicine, electromagnetics, and science (Aljerf and Nadra 2019). In its environmental applications, magnetite nanoparticles are used to facilitate separation of sorbent from drinking water and wastewater due to their effective and easily separation features (Sharma et al. 2018). However, it is known that the coaggregation problem of nanoparticles is often difficult to overcome because the coaggregation reduces the effective surface area of the nanoparticles resulting in reduced reaction activity (Mittal 2013). In order to solve the problem, magnetic nanoparticles were prepared as a nanocomposite supported by olive pomace (Abdolmohammad et al. 2019). Development of magnetized magnetic biosorbents is of importance for more efficient and easier separation in the sorption process, since the active surface of the magnetite particles is attached to the polymeric structure and becomes an important adsorbent to remove heavy metals (Khorasani and Shojaosadati 2019). For sorption of cerium(III) from aqueous solutions, most researchers have used different materials, natural, organic, and inorganic: *Platanus orientalis* leaf powder (Ser et al. 2008), montmorillonite (Klika et al. 2016), ferric oxide (Dubey and Rao 2011), tangerine (Citrus reticulate) peel (Torab-Mostaedi, 2013), granulated zeolites (Suboti and Bronic 1986), and brown marine alga (Vijayaraghavan et al. 2010). To the best of our knowledge, the study is the first to show that a magnetic nanocomposite of olive pomace and magnetite is used to adsorb cerium ions from aqueous solutions.

The utilization of agro-wastes as adsorbents is currently receiving wide attention because of their abundant availability and low cost owing to relatively high fixed carbon content and presence of porous structure [8,9]. In economic terms, it is very important to dispose this material obtained as waste from the olive oil production (Khdair and Abu-Rumman 2020). For such reasons, removal of toxic cerium ions from aqueous solutions is very vital for human and environment health. Therefore, nanocomposite was prepared using magnetic nanoparticles and olive pomace which are inexpensive (with a cost of less than 50$/ton against 4500$/ton of a granular activated carbon) and less toxic (Pagnanelli et al. 2003). However, a magnetic olive pomace nanocomposite (MOP) has not been investigated as an adsorbent for cerium in the literature. Therefore, in this study, synthesis was conducted by partial reduction co-precipitation which is a simple, effective, and economical and environment friendly technique. Adsorbents were then characterized by scanning electron microscopy (SEM), transmission electron microscopy (TEM), Fourier transform infrared spectroscopy (FT-IR), vibrating sample magnetometry (VSM), and surface area measurements (BET). The effects of various operational parameters on the sorption efficiency for the Ce(III) ions were also studied. Finally, the sorption isotherm models, kinetics, and thermodynamics were studied as parameters influencing the sorption capacity and sorption process.

Materials and methods

Reagents and materials

The chemicals used are iron(III) chloride ($FeCl_3$, Fluka), sodium sulfite (Na_2SO_3, Merck), hydrochloric acid (HCl, Merck), ammonia (NH_3, Merck), and ethanol (C_2H_5OH, Merck). 3.09 ±0.01 g of $Ce(NO_3)_3{\cdot}6H_2O$ (Merck) was dissolved separately in 1 L of distilled water to prepare the stock solution of cerium with a concentration of 1000 mgL^{-1}. Other concentrations ranging from 25 to 300 mgL^{-1} were prepared by diluting the initial stock solutions with double distilled water. The pH was adjusted by diluted solutions of HNO_3 and NH_4OH. All the chemical reactants were used as analytical grade (AR).

The olive pomace extracted using hexane was obtained from the Ege Tarımsal Enerji San. ve Tic. A.Ş., Torbalı, Izmir, Turkey. Then olive pomace was washed by distilled water, dried at room temperature, and grounded using a grinding mill to obtain 25 mm in particle size. Then 10 g of raw olive pomace (OP) was added to 100 mL of 1 M H_3PO_4 solution which was stirred by mechanical stirrer for 24 h. After the mixing was completed, the solution was washed with distilled water to eliminate the chemical agent excess until the pH reached to neutral, and the samples were dried in an oven at 60 °C and after stored for later use.

Instrument

Determination of Ce(III) in aqueous solutions was conducted using inductively coupled plasma optical emission spectrometry (ICP-OES) (Perkin Elmer Optima DV 2000). The pH values of all solutions were measured by a Hanna Instrument, model 8521, pH meter. The SEM images were obtained at 5.0 kV on a field emission scanning electron microscope (Philips XL 30S FEG). Studies of the transmission electron microscopy (TEM) were performed using Jem Jeol 2100F 200kV HRTEM under the 200kV and FEI Tecnai G^2 Spirit Bio (TWIN) CTEM under the 120kV. FT-IR spectra were recorded in the 4400–400 cm^{-1} spectral region by means of a Thermo FT-IR spectrometer. Magnetic measurements of the samples in the powder form were carried out at room temperature using a vibrating sample magnetometry (VSM)

(Lakeshore 7407). N_2-BET adsorption–desorption was determined using Micromeritics ASAP 2020 equipment at 77 K, for specific surface area and porosity evaluation for magnetic nanoparticles and magnetic olive pomace nanocomposite. The adsorption experiments were studied by batch technique using a thermostated shaker water bath, model GFL-1083.

Synthesis of magnetic nanoparticles and nanocomposite

The magnetic nanoparticles (MNP) and magnetic olive pomace (MOP) nanocomposite were prepared by partial reduction co-precipitation, as reported in the literature (Yusan et al. 2014).

The olive pomace sample was chemically modified with phosphoric acid (H_3PO_4) as follows: 10 g raw olive pomace was added to 100 mL of 1 M H_3PO_4 in which the solution was stirred with mechanical stirrer for 24 h. After the mixing was completed, the solution was washed with distilled water to eliminate the chemical agent excess until the pH reached neutral, and the samples were dried in an oven at 60 °C and after stored for later use. One gram of modified (with phosphoric acid) olive pomace was used in the synthesis of the nanocomposite.

Firstly, N_2 gas was bubbled through distilled water used in synthesis to remove dissolved oxygen for 5 min. To prepare the magnetic olive pomace nanocomposite, $FeCl_3$ was dissolved in 2.0 M HCl and transferred to a 500-mL three-neck flask and diluted with 100 mL distilled water. Later, freshly prepared 0.08 M Na_2SO_3 was added slowly under nitrogen atmosphere. Afterwards, 1.0 g of modified olive pomace was poured into the three-neck flask with a mixture of 3.0 M 6.0 mL of iron chloride solution in it. Eight milliliters of NH_3 solution (28%, w/v) was gently added to the mixture under nitrogen atmosphere and then diluted with distilled water (25 mL). The solution was later allowed to stand at 70 °C for 15–30 min, and black precipitate was collected with a magnet and washed by distilled water until the pH of the suspension reached to 7.0 and then continued to wash with water–ethanol (2/1, v/v) mixture. The precipitate was dried at vacuum in 45 °C and used for the characterization.

Sorption experiments

Sorption was carried out in thermostatic water bath shaker using 10 mL of Ce(III) solutions at the appropriate concentrations and 0.04 g of adsorbent by batch technique. The effects of sorption parameters such as contact time (5–240 min), pH (1–6), Ce(III) concentration (25–300 mgL^{-1}), and temperature (30–50 °C) on the sorption of Ce(III) were determined by changing one parameter and keeping others constant. After sorption, the solution was vacuum filtered through the membrane filters, and the Ce(III) concentrations in the solutions were determined using the ICP-OES instrument. Solutions of 10, 25, 50, and 100 mgL^{-1} Ce(III) concentration and 150, 250, and 300 mgL^{-1} for higher concentrations were used as standard for calibration in ICP-OES instrument.

The isothermal studies were performed by changing the initial cerium concentration from 25 to 300 mgL^{-1}, while the rest of the parameters were kept at their optimal values.

The sorption kinetics were realized at 50 mgL^{-1} cerium concentration from 5 to 240 min contact time at 25 °C. The sorption capacity of Ce(III) ions sorbed per gram sorbent (qe, mgg^{-1}) and sorption efficiency (Sorp.%), according to the obtained data, are calculated in the following:

$$Sorption(\%) = \frac{(C_0 - C_e)}{C_e} \times 100 \quad (1)$$

$$q_e = \frac{(C_i - C_e)V}{W} \quad (2)$$

C_0 is the initial concentration of adsorbate (mgL^{-1}); C_e is the equilibrium concentration of adsorbate (mgL^{-1}); W is the mass of the adsorbent (g); and V is the volume of the aqueous phase (mL). All the experiments were performed in duplicates with experimental errors within ±3%.

Results and discussion

Characterization

The morphology of magnetic olive pomace was analyzed by SEM in Fig. 1. Surface image of MOP showed agglomeration of spherical shaped Fe_3O_4 nanoparticles with varying sizes. It can be concluded that Fe_3O_4 nanoparticles are attached to the surface of the olive pomace.

Figure 2A and B illustrate the TEM images of magnetite and magnetite-olive pomace nanocomposite, respectively. They show that magnetite-olive pomace nanocomposite was being more uniform than pure magnetite nanoparticles. And also Fig. 2 B indicates that Fe_3O_4 nanoparticles are well decorated and clearly observed. Due to filling of magnetite particles aggregate with olive pomace, the specific surface area of nanocomposite decreased (Pylypchuk et al. 2016).

Brunauer-Emmett-Teller (BET) analysis was performed to investigate the specific surface area of the magnetic nanocomposite. The BET surface area of the nanocomposite was found to be 120.37 m^2 g^{-1}. The literature found surface area of pure magnetite between 134 and 286.9 m^2 g^{-1} (Pylypchuk et al. 2016; Ardelean et al. 2017; Ma et al., 2014). Moreover, the surface area of the raw olive pomace was measured as 0.90 m^2 g^{-1}, according to which the surface area of the nanocomposite formed by magnetite with olive pomace can be concluded to be significantly increased.

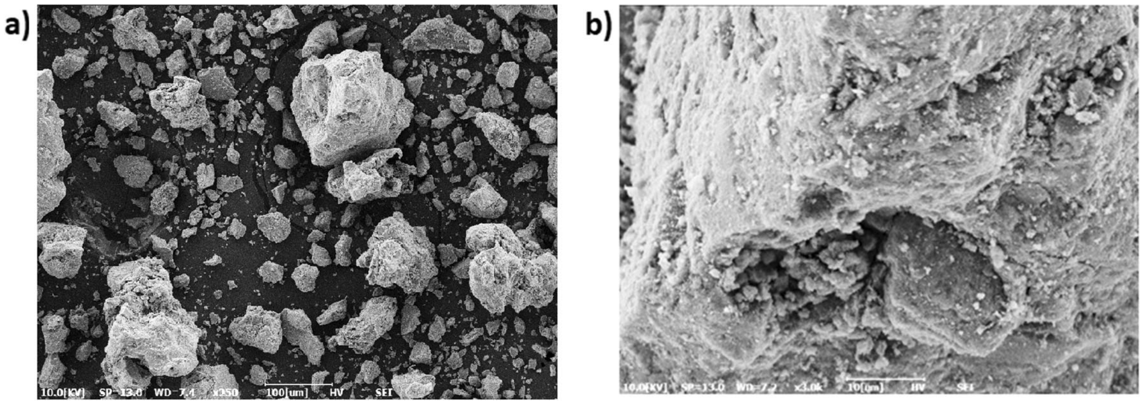

Fig. 1 SEM images of magnetite-olive pomace nanocomposite (MOP) with various magnifications

The FT-IR spectra of MNP and MOP are described in Fig. 3.In addition, the previous study showed that olive pomace and modified olive pomace spectra were provided to see the difference of the adsorbents (Akbas and Yusan 2020). From the Fig. 3, MNP vibration modes appeared at 3552.20 cm^{-1}, and 1633.88 cm^{-1} and 890.97 cm^{-1} are assigned to the vibrations of hydrogen-bonded water molecules adsorbed on the surface and O-H bending vibration, and additional band was found at 1433.36 cm^{-1} for C-O vibration modes (Ahmadi et al. 2020). The band at 550.34 cm^{-1} was associated to the Fe-O vibration characteristic of the magnetite phase, which was the main band for both spectra (Karimzadeh et al. 2017).

The main bands for MOP could be assigned at about 3322.05 cm^{-1} (OH and NH_2 stretching vibrations), 2924 cm^{-1} (C–H stretch vibration of the of CH, CH_2 and CH_3 groups), 1637 cm^{-1} (OH and NH_2 bending vibration), 1230 cm^{-1} (antisymmetric stretch C–O–C and C–N stretch vibration), 1032 cm^{-1} (C–O stretch vibration), and 522 cm^{-1} (Fe-O vibration). From the Fig. 3, it follows that Fe-O band shifted from 550 to 552 cm^{-1} after the formation of the nanocomposite (Iconaru et al. 2016).

The magnetic properties of the magnetite nanoparticles and magnetic olive pomace nanocomposite were determined at room temperature (Taufiq et al. 2017). According to VSM results from Fig. 4, saturation magnetization was found 20.13 and 16.15 emug^{-1} for the magnetite and magnetic nanocomposite, respectively. It can be concluded that both sorbents are superparamagnetic. The magnetization value for magnetite-olive pomace nanocomposite was less than magnetite nanoparticles due to the presence of olive pomace onto the body of nanoparticles. Although magnetization of nanocomposite in the saturation was lower than magnetite, magnetic separation of MOP was still rapid.

The XRD analysis was also used to determine the crystalline structure of the material, whose results for the MNP and MOP composite are shown in Fig. 5. In the MNP, the peaks at 2θ values of 30.2; 35.4; 43.3; 53.5; 57.2; and 63.0 are quite identical to characteristic peaks of the Fe_3O_4 crystal with the cubic spinal structure for magnetic olive pomace composite

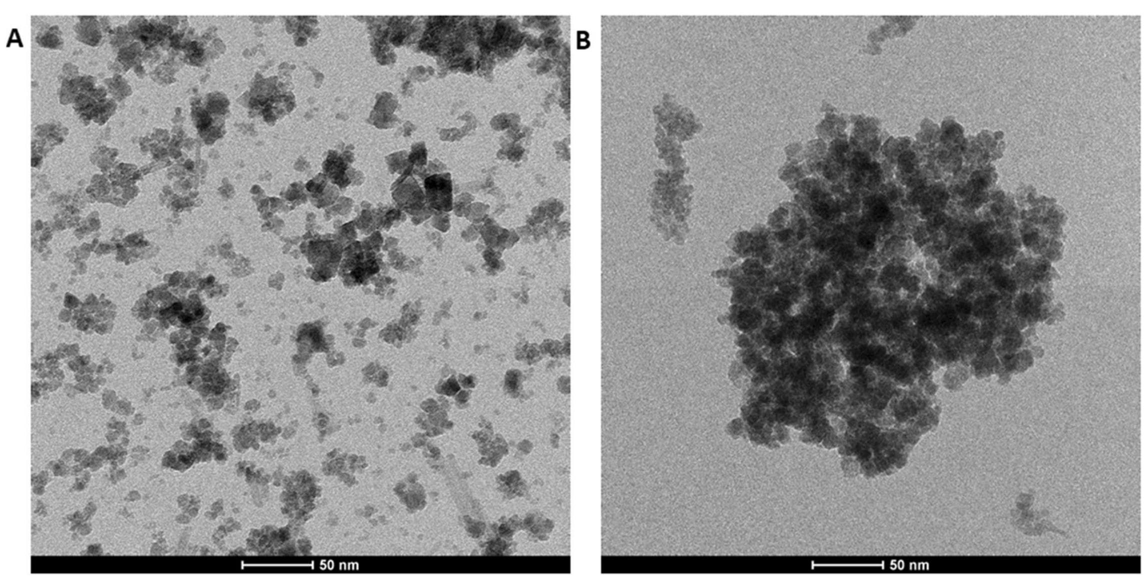

Fig. 2 TEM images of MNP (**A**) and MOP (**B**)

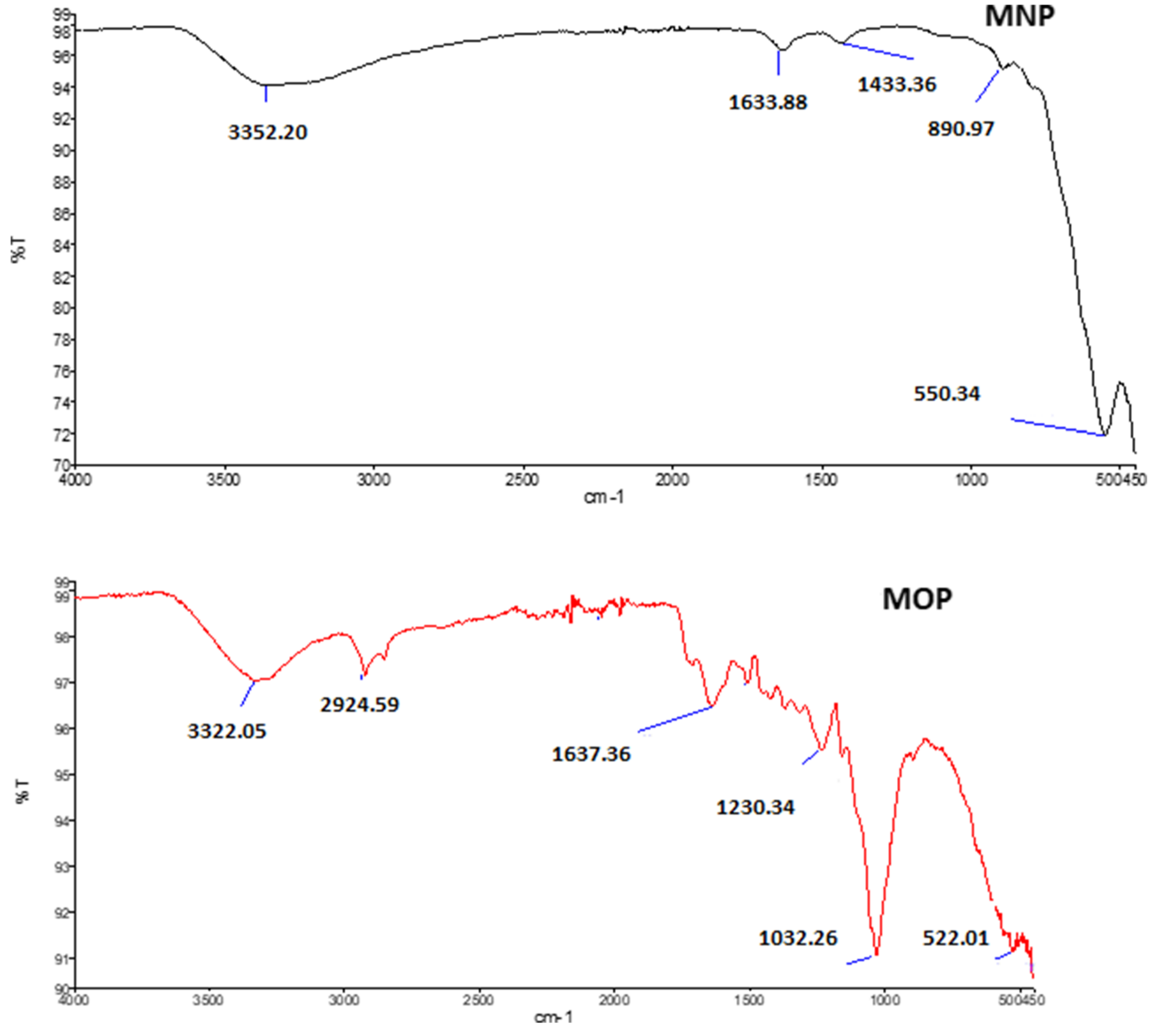

Fig. 3 FT-IR spectra of MNP and MOP

which is in good agreement with the value in the literature (JCPDS card No. 19-0629) (Yusan et al. 2014; Boushehrian et al. 2020; Azari et al. 2017) which are marked by 220, 311, 400, 422, 511, and 440 indices, respectively. After the formation of magnetic olive pomace composite, the intensities of the peaks for composite were decreased, and composite structure was not in a good crystalline form due to the olive pomace incorporation.

Fig. 4 Hysteresis loops of the MNP and MOP

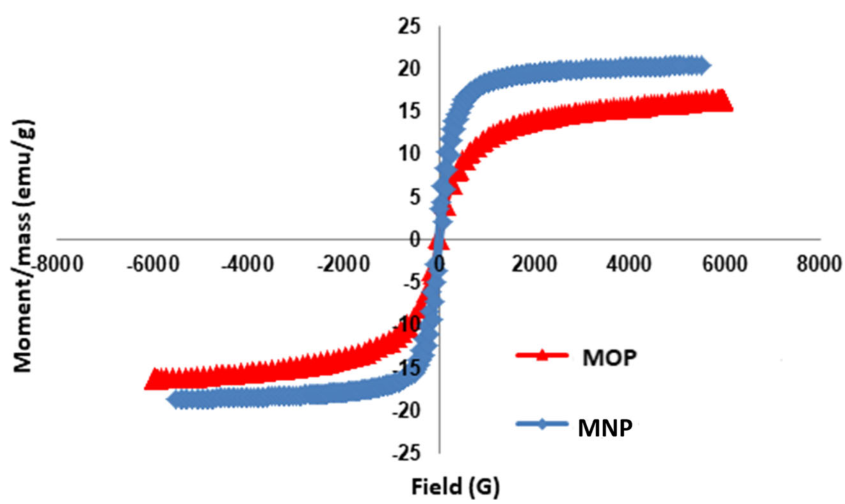

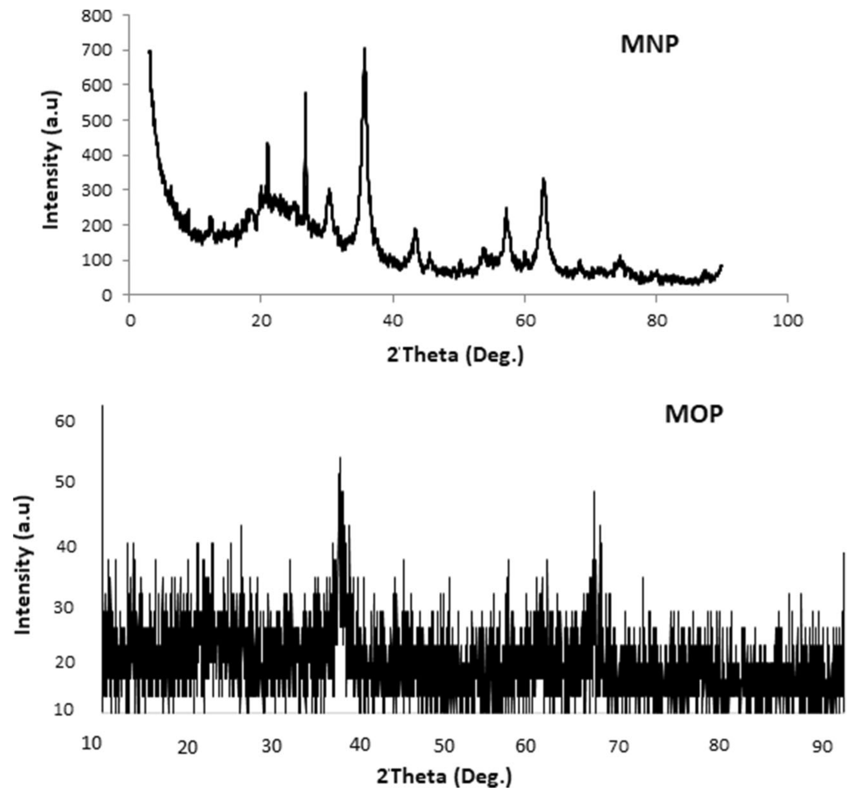

Fig. 5 XRD pattern of the MNP and MOP

Sorption experiments

Effect of pH

The solution pH plays a major role in the removal of adsorbents from aqueous solutions since its effect on the surface charge of the adsorbent, the degree of ionization, and the speciation of adsorbate and surface functional groups influence the sorption process (Aljerf 2018). The impact of pH on the sorption capacity of synthesized materials was studied using solution of 100 mgL^{-1} Ce(III) at a pH range of 1.0–6.0 (at pH >6.5, Ce(III) ions precipitated) at 25 °C for 120 min (Iconaru et al. 2016; Kutahyalı et al. 2012). The results of the experiment are in Fig. 6. As seen from Fig. 6, maximum Ce(III) uptake was obtained at pH 6.0 for magnetite (MNP) and magnetite-olive pomace nanocomposite (MOP) as 12.22 mgg^{-1} and 13.93 mgg^{-1}, respectively. The results from Fig. 6 suggested that the sorption capacity of MOP was better than MNP which could be associated with the lignocellulosic structure of the olive pomace.

Effect of contact time

Contact time is an important parameter for investigation of the sorption process (Aljerf 2018). The sorption experiments were

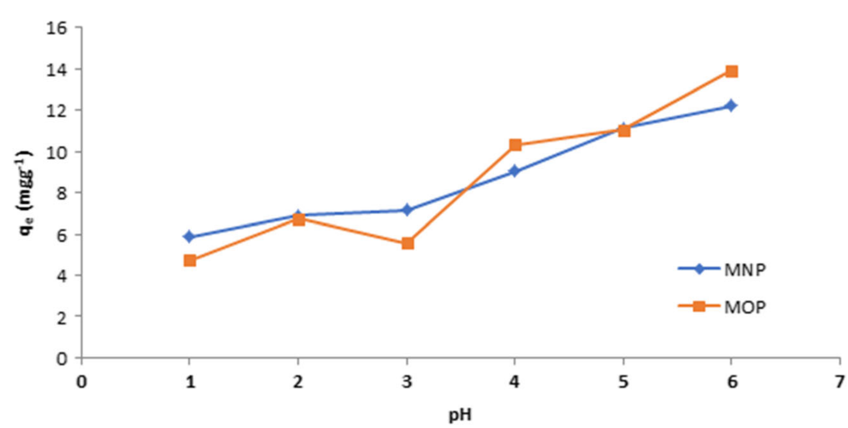

Fig. 6 Influence of pH on sorption of Ce(III) ions by the MNP and MOP nanocomposite (m: 0.04 g, c: 100 mgL^{-1}, v: 10 mL, t: 2 h)

carried out for contact times ranging from 5 to 240 min with fixed amounts of adsorbent (0.04 g) at ambient temperature (25 °C) with all other parameters kept constant (Fig. 7).

As seen from Fig. 7, sorption was initially fast and occupied selectively the active sites on the adsorbents. The active sites on the adsorbents were filled when the contact time was increased and the sorption of Ce(III) onto adsorbents reached to an equilibrium (Gunasundari et al. 2017; Pearlin et al. 2014). For further experiments, the optimum contact time was selected 30 and 45 min for MNP and MOP, respectively.

Effect of initial Ce(III) concentration

The influence of the Ce(III) concentration on adsorption was investigated in a range from 25 to 300 mgL^{-1}. The results are exhibited in Fig. 8. The sorption capacities of cerium(III) by MNP and MOP were found 6.20 mgg^{-1} and 12.57 mgg^{-1}, respectively. The higher sorption capacity of the MOP might be contributed to by cellulose, hemicellulose, and lignin contents of the magnetic nanocomposite. For both sorbents, sorption capacity increases with the Ce(III) initial concentration, and then they reach an equilibrium, which can be explained by the theory that the mass transfer driving force at the solid-liquid interface is enhanced as the initial concentration increases.

Thermodynamic studies

Figure 9 shows the effect of temperature and thermodynamic features on the sorption of cerium on the MNP and MOP nanocomposite. Thermodynamic parameters such as changes of enthalpy (ΔH°), entropy (ΔS°), and free energy (ΔG°) were estimated by the following and given in Table 1.

$$lnK_d = \frac{\Delta S^o}{R} - \frac{\Delta H^o}{RT} \tag{3}$$

$$\Delta G^o = \Delta H^o - T\Delta S^o \tag{4}$$

Analysis of thermodynamic parameters does not only judge the nature of adsorption process but also provides the information on predominant mechanisms in the adsorption reaction (e.g., physical interaction, chemical interaction) (Yan et al. 2020). The positive value of the enthalpy change suggests the endothermic nature of the sorption process for MNP and MOP. The positive value of Δ^{0} due to the exchange of the Ce(III) ions with more mobile ions present on the exchanger would lead to increase the entropy in the sorption process (Tamjidi et al. 2019). The positive values of Δ^{0} suggested that Ce (III) sorption at various temperatures was thermodynamically non-spontaneous in nature for the both sorbents (Ahmad et al. 2011; Haroon et al. 2016; Yi et al., 2017; Sangkarak et al. 2020). ΔH° and ΔS° values were positive, confirming that adsorption system of Ce(III) onto the MNP and MOP at the test temperatures was endothermic. It was expected that the degree of randomness at the solid–liquid interface would increase during the adsorption system. Moreover, similar evidence was found for the heavy metal adsorption (Haroon et al. 2016; Sangkarak et al. 2020; Schneider et al. 2007). When the value of ΔH° is lower than 40 $kJmol^{-1}$, the type of sorption can be accepted as a physical process. The values of ΔH° were calculated as 5.7872 $kJmol^{-1}$ and 7.4495 $kJmol^{-1}$ for MNP and MOP, respectively. They indicate that the sorption was physical by nature and thus involved weak forces of attraction (Ho and McKay 1999), which is consistent with the results of the isotherm models. Furthermore, uptake of cerium can be concluded to be slightly increases at temperature increased (Kaveeshwar et al. 2018).

Adsorption isotherms

The Langmuir, Freundlich, and Dubinin-Radushkevich (D-R) isotherm models were applied to obtain data of Ce(III) sorption mechanism on MNP and MOP nanocomposite surface. Linear and non-linear regression methods were compared to determine the best fitting of isotherm to experimental data. Non-linear regression was performed using trial and error

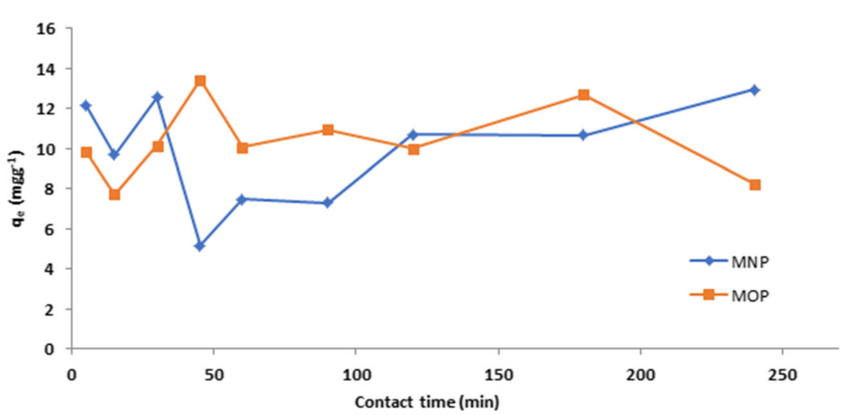

Fig. 7 Influence of contact time on sorption of Ce(III) ions by the MNP and MOP nanocomposite (MNP: m: 0.04 g, v: 10mL, pH:6.0 and c:100 mgL^{-1}, MOP: m: 0.04 g, v: 10 mL, pH: 6.0 and c: 100 mgL^{-1})

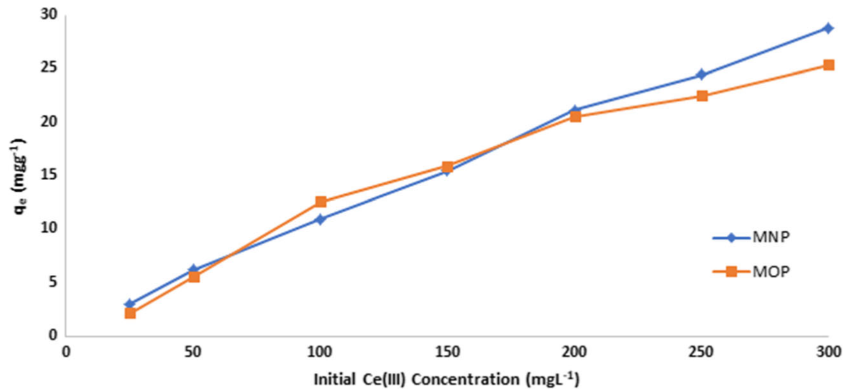

Fig. 8 Influence of initial concentration of Ce(III) ions by the MNP and MOP nanocomposite (MNP: m: 0.04 g, v: 10mL, pH:6.0 and t: 30 min, MOP: m: 0.04 g, v: 10 mL, pH: 6.0 and t: 45 min)

method with the help of solver add-in functions of Microsoft Excel software. An error function assessment is required in order to evaluate the fit of the equation to the experimental results. The coefficient of determination (R^2) was used in order to find the fitting degrees of isotherm with experimental data in this study (Foo and Hameed 2010).

$$R^2 = \frac{\sum\left(q_{e,exp} - \overline{q_{e,cal}}\right)^2}{\sum\left(q_{e,exp} - \overline{q_{e,cal}}\right)^2 + \sum\left(q_{e,exp} - q_{e,cal}\right)^2} \quad (5)$$

where $q_{e,exp}$ is the amount of metal ions biosorbed onto biosorbent obtained from experiment, $q_{e,cal}$ is the amount of metal ions obtained by isotherm models, and $q_{e;cal}$ is the average of $q_{e,exp}$. The isotherm equations and the results are presented in Tables 2 and 3, respectively. The calculated maximum capacity (mgg^{-1}) expresses the total capacity of the sorbent for cerium, and the R_L values were calculated within the range of 0–1 confirming the favorable character of the uptake of the cerium by the adsorbents (Anitha et al. 2015). Table 3 shows that D-R isotherm model (0.9981) was very suitable for describing the sorption equilibrium of cerium by the magnetic olive pomace nanocomposite. Otherwise, Freundlich isotherm model (0.9944) and D-R isotherm model (0.998) are fitted very well for MNP. Therefore, it can be inferred that the sorption process followed both isotherm models. According to the affinity of the interaction between adsorbent and adsorbate can be explained by the value of the sorption intensity (n) by the Freundlich isotherm model, the value 1 < n < 10 illustrates that sorption tends to be favored. The importance of n is given as follows: n < 1 (chemical process); n = 1 (linear); n > 1 (physical process) (Saravan et al. 2018). As seen from the Table 3, n values are in the same range for both of the sorbent, and n value is higher than 1. Accordingly, it can be concluded that physical sorption is favorable for both adsorbents.

q_{eq}, C_{eq} equilibrium concentrations of cerium in solid and liquid phase, respectively; Q_o is the maximum sorption capacity (mgg^{-1}); b_L is the Langmuir constant related to sorption energy. K_F is the sorption capacity of sorbent (mgg^{-1}), and n_F is a constant related to sorption intensity (dimensionless) for Freundlich isotherm model. C_{ads} (molg^{-1}) is the amount of solute sorbed per unit weights of solid, X_m (molg^{-1} or mgg^{-1}) is the sorption capacity, β (molJ^{-1})^2 is a constant related to energy, and $\mathcal{E}$ is the Dubinin-Radushkevich isotherm constant. This approach is generally used to distinguish whether the physical and chemical adsorption of metal ions is by the mean free energy, E per molecule of adsorbate, which can be calculated by the relationship (Dada et al. 2012).

Non-linear regression exhibited higher coefficient of determination value for Langmuir isotherm than the linear regression for MNP and MOP. The maximum monomolecular sorption capacity (qmax) of MNP and MOP obtained from non-

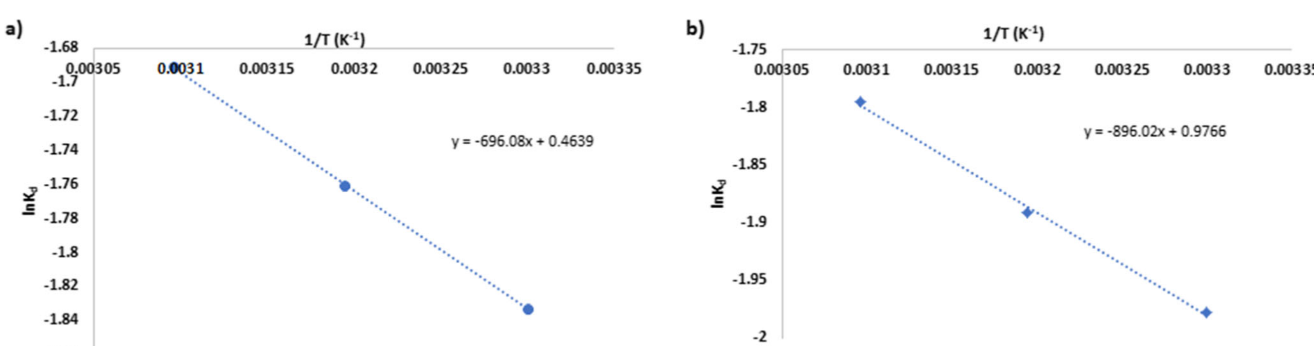

Fig. 9 $\ln K_d$ versus temperature graph of Ce(III) sorption by the MNP (**a**) and MOP (**b**) nanocomposite

Table 1 Thermodynamics parameters of Ce(III) sorption

Sorbent	ΔH° (kJ/mol)	ΔS° (J/molK)	ΔG° (kJ/mol)		
			303 K	313 K	323 K
MNP	5.7872	0.0039	4.6186	4.5800	4.5414
MOP	7.4495	0.0081	4.9893	4.9081	4.8269

linear regression was found to be 100.53 mgg^{-1} and 93.984 mgg^{-1} for cerium, respectively. When the linear and non-linear isotherm models were compared, it was seen that the constants and regression values of the models except the Langmuir isotherm model were compatible with each other.

Comparison of non-linear isotherm models with experimental data of cerium sorption onto MNP and MOP is shown in Fig. 10.

Using the linear plot of D-R isotherm model, X_m was determined to 0.0050 and 0.0053 $molg^{-1}$, the mean free energy, E= 7 $kJmol^{-1}$ and 6.93 $kJmol^{-1}$ for MNP and MOP, respectively. These results indicate physiosorption process for both sorbents (Kumar et al. 2011).

Unfortunately, there is no related information about Ce(III) sorption on magnetite-olive pomace nanocomposite. Sorption capacities of the MNP and MOP nanocomposite can be compared with those of sorbents in the literature for Ce(III) sorption (Table 4). The results below indicate that the maximum sorption capacities from the study can be comparable with those in the literature ranging from 12.08 to 180.2 mgg^{-1} for Ce(III).

Adsorption kinetics

The present study used two kinetic models to investigate the mechanism of sorption and rate-controlling processes, such as mass transfer and/or chemical reaction. The linear forms of the pseudo-first-order and pseudo-second-order equations are in the following equations, respectively:

$$\log(q_e - q_t) = log q_e - \frac{k_1 t}{2.303} \quad (6)$$

$$\frac{t}{q_t} = \frac{1}{k_2 q_e^2} + \frac{t}{q_e} \quad (7)$$

where q_e and q_t (mgg^{-1}) are the amounts of adsorbate adsorbed at equilibrium and at any time; t (h), k_1 (1/h), and k_2 (g mgh^{-1}) are the equilibrium rate constants of pseudo-first-order and pseudo-second-order models; and t (h) is the contact time, respectively.

In the present work, the kinetic experiments of Ce(III) sorption onto MNP and MOP were analyzed using the pseudo-first-order (not shown) and pseudo-second-order kinetic models with results in Fig. 11.

The linear plot of log (q_e - q_t) versus t provides a slope of k_1 and intercept of log q_e. The values of k_1 and R^2 from the plot for sorption of Ce(III) on the adsorbents are shown in Table 5.

According to the kinetic models, the calculated constants for the sorption kinetics are in Table 5. The R^2 values for the pseudo-first-order model for both adsorbents were not high, which shows that the sorption of Ce(III) on the adsorbents does not follow a pseudo-first-order kinetic model. Based on Table 5, R^2 values obtained from the pseudo-second-order model were high, and q_e values are in good agreement with the experimental results. It is clear that the sorption of Ce(III) on MNP and MOP fits this model well and sorption process is controlled by different sorption mechanisms, such as surface complexation and ion exchange (Alslaibi et al. 2013; Lazarević et al. 2010; Hubbe et al. 2019).

Conclusion

In this study, magnetic olive pomace (MOP) nanocomposite was successfully synthesized, characterized, and used for the adsorption of Ce(III) ions from an aqueous solution. According to the results, optimum operation conditions were determined as pH of 6.00, at 45-min contact time, 100 mgL^{-1} Ce(III) concentration, and 40 °C and pH of 6.00, at 30 min contact time, 50 mgL^{-1} Ce(III) concentration, and 40 °C for MOP and MNP, respectively. The maximum sorption capacities of MNP and MOP for Ce(III) were found to be 76.92 mgg^{-1} and 90.90 mgg^{-1}, respectively. They were comparable/acceptable with the previous reported adsorbents for Ce(III)

Table 2 Utilized isotherms models (linear) in sorption studies

Name	Linear equation	Non-linear equation
Langmuir	$\frac{C_e}{q_e} = \frac{1}{Q_o b_L} + \frac{C_e}{Q_o}$ $R_L = \frac{1}{1+b_L C_o}$	$q_e = \frac{Q_0 b_L C_e}{1+b_L C_e}$
Freundlich	$\log q_e = \log K_F + \frac{1}{n_F} \log C_e$	$q_e = K_F X C_e^{1/n}$
Dubinin-Radushkevich	$\ln C_{ads} = \ln X_m - \beta\varepsilon^2$ $\varepsilon = RTln\left(\frac{1}{1+C_e}\right)$ $E = \frac{1}{\sqrt{-2\beta}}$	$C_{ads} = X_m e^{-\beta e2}$

Table 3 Constants of linear and non-linear isotherm models

		Linearized isotherm		Non-linearized isotherm	
Isotherm models	Parameters	MNP	MOP	MNP	MOP
Langmuir	q_{max} (mg/g)	76.9231	90.9091	100.53	93.984
	b_L (L/mg)	0.0031	0.0022	0.0023	0.0024
	R_L	0.7040	0.7674	0.635	0.581
	R^2	0.9002	0.2774	0.9979	0.9777
Freundlich	K_F (mg/^{1})	2.6634	0.2103	0.885	0.232
	n	1.1952	1.0787	1.495	1.063
	R^2	0.9944	0.9291	0.9976	0.9615
Dubinin-Radushkevich	X_m (mol/g)	0.0050	0.0053	0.0049	0.0052
	E (kJ/mol)	7.00	6.9300	6.99	6.94
	R^2	0.998	0.9981	0.9989	0.9981

removal. According to the results of the equilibrium study, one can infer that the cerium ion adsorption on the studied adsorbents is a favorable physical process where the equilibrium data follows the D-R and Freundlich isotherm models. In

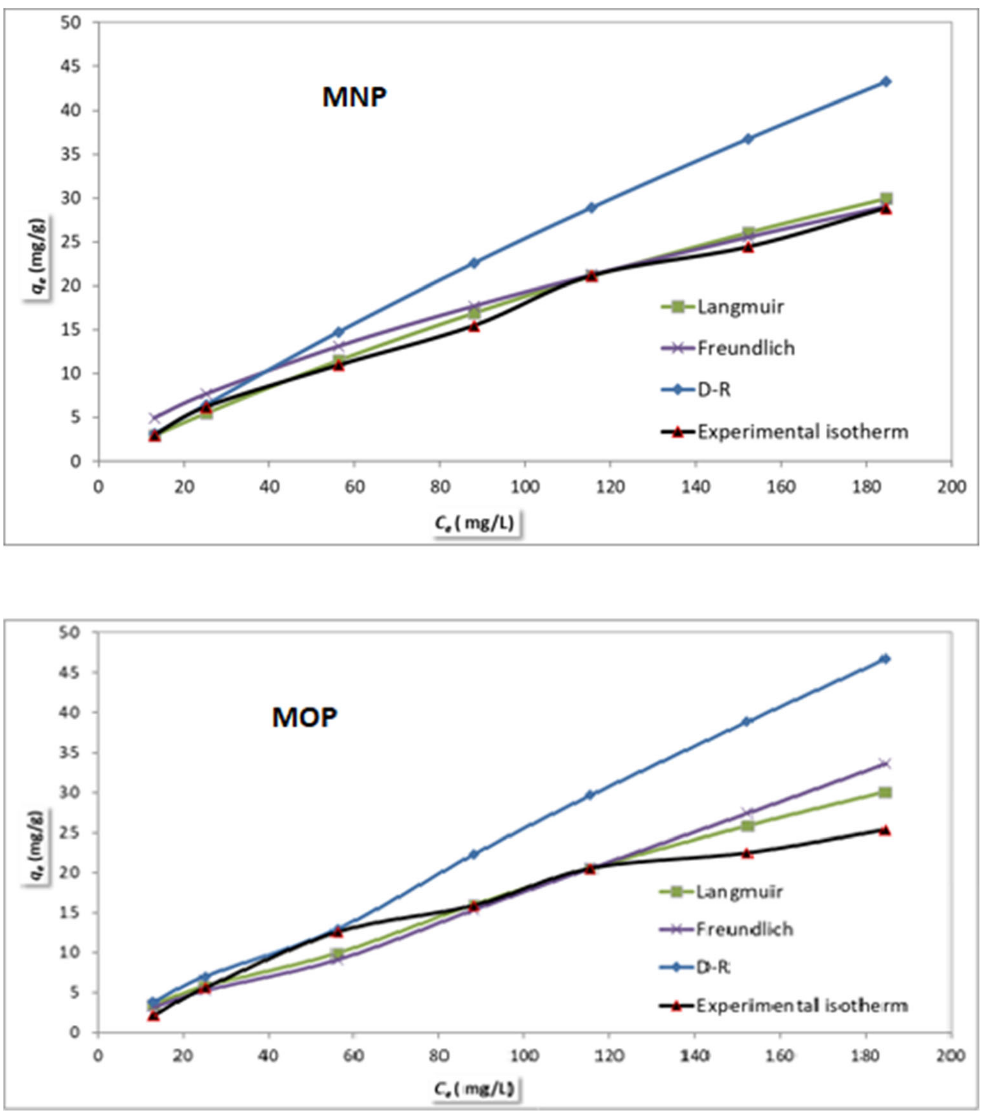

Fig. 10 Comparison of non-linear isotherm models with experimental data of cerium sorption onto MNP and MOP

Table 4 Comparative of Ce(III) capacities with the literature

Adsorbent	Sorption capacity (mgg^{-1})	Reference
Modified *Pinus brutia* leaf powder	62.1	Kutahyalı et al. (2012)
Pinus brutia leaf powder	17.2	Sert et al. (2008)
Brown marine alga	152.8	Vijayaraghavan et al. (2010)
Crab shell	144.9	Vijayaraghavan and Balasubramanian (2010)
Multi walled carbon nanotubes	92.59	Behdani et al. (2013)
Prawn carapace (PC)	218.3	Varsihini et al. (2014)
Corn style (CS)	180.2	Varsihini et al. (2014)
Grapefruit peel	159.30	Torab-Mostaedi et al. (2015)
CRAC	94.34	Chen et al. (2015)
Endemic type (ES)	18.1	Sadovsky et al. (2016)
Commercial powder (CS)	38.2	Sadovsky et al. (2016)
Alg-Fe_3O_4 nanoparticles	31.83	Serunting et al. (2018)
SBA-15 mesoporous silica	26.67	Dorabei et al. (2016)
Unmodified nano TiO_2	12.08	Shojaei et al. (2016)
Modified nano TiO_2	21.39	Shojaei et al. (2016)
MNP	76.92	Present study
MOP nanocomposite	90.90	Present study

the meantime, according to results from the kinetic and thermodynamic study, the sorption process is controlled by different sorption mechanisms, such as surface complexation, ion exchange, and electrostatic attraction which are the contributions to the effective removal of Ce(III) ions.

The SEM and TEM pictures showed magnetic particles located on the olive pomace surface. The BET surface area of the nanocomposite was found as 120.37 m^2g^{-1}. According to VSM results, MNP and MOP were superparamagnetic and saturation magnetization 20.13 and 16.15 $emug^{-1}$.

From the study, it was clear that magnetite/olive pomace nanocomposite could be an effective biosorbent for Ce(III) removal from aqueous media, based on which synthesized adsorbents have good magnetic property related to the magnetic field for easy removal of adsorbent from the aqueous solutions. Therefore, it can be considered that these adsorbents can be used as an effective one to effectively remove Ce ions from wastewater.

Acknowledgements We would like to express our deep gratitude to Dr. Berkan Cetinkaya and Dr. Emine Nostar Aslan for BET and FT-IR analysis in Ege University Institute of Nuclear Sciences.

Author contribution Yusuf Azmi Akbas: Synthesis of the materials, realization of the experiments, calculations

Sabriye Yusan: Supervision, data acquisition, methodology, and writing - review and editing

Senol Sert: Measurements of the Ce ions by ICP-OES

Sule Aytas: Data analysis and writing - review and editing

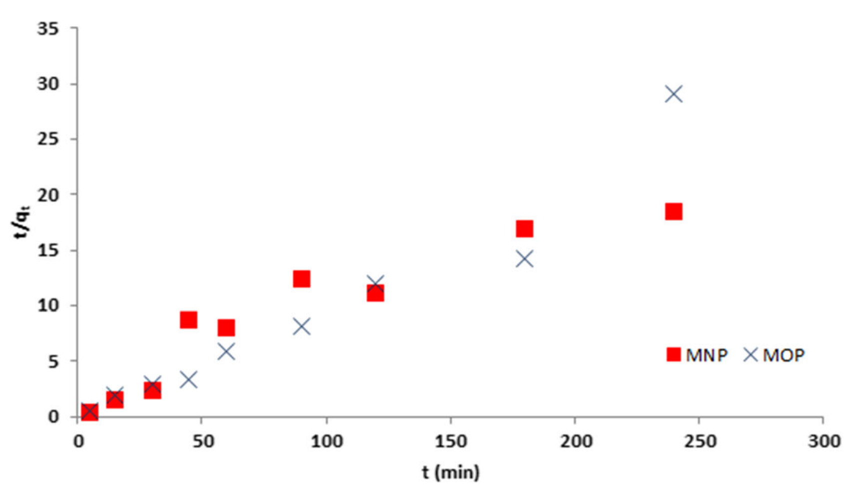

Fig. 11 Plot of pseudo-second-order kinetic model for sorption of Ce(III) onto MNP and MOP

Table 5 Kinetic parameters of pseudo-first- and pseudo-second-order models for the sorption of Ce(III) onto MNP and MOP

Adsorbent	MNP	MOP
Pseudo-first-order kinetic model		
q_e (mg/g)	3.2018	0.7252
k_1 (1/min)	0.0151	0.0032
R^2	0.3671	0.1387
Pseudo-second-order kinetic model		
q_e (mg/g)	12.9366	9.1996
k_2 (g /mol min)	0.0027	0.0149
R^2	0.8864	0.9392
Experimental q_e (mg/g)	12.8625	10.0091

Funding This study was financially supported by the Ege University Scientific Research Project Unit Project No. 2016 NBE 002.

Data availability The datasets used and/or analyzed in this study are available from the corresponding author on reasonable request (sabriyeyusan@gmail.com).

Declarations

Ethical approval Not applicable: our manuscript does not report on or involve the use of any animal or human data or tissue.

Consent to participate Not applicable

Consent to publish Not applicable

Conflict of interest The authors declare no competing interests.

References

Abdolmohammad-Zadeh H, Ayazi Z, Naghdi Z (2019) Nickel oxide/chitosan nano-composite as a magnetic adsorbent for preconcentration of Zn(II) ions. J Magn Magn Mater 488:165311

Ahmad MA, Rahman NK (2011) Equilibrium, kinetics and thermodynamic of Remazol Brilliant Orange 3R dye adsorption on coffee husk-based activated carbon. Chem Eng J 170:154–161

Ahmadi A, Foroutan R, Esmaeili H, Tamjidi S (2020) The role of bentonite clay and bentonite clay@MnFe2O4 composite and their physico-chemical properties on the removal of Cr(III) and Cr(VI) from aqueous media. Environ Sci Pollut Res 27:14044–14057

Ajinkya N, Yu X, Kaithal P, Luo H, Somani P, Ramakrishna S (2020) Magnetic iron oxide nanoparticle (IONP) synthesis to applications: present and future. Materials 13(20):4644

Akbas YA, Yusan S (2020) Development and characterization of non-treated and chemically modified olive pomace biosorbents to remove Ce(III) ions from aqueous solutions. J Radioanal Nucl Chem 323:763–772

Aljerf L (2018) High-efficiency extraction of bromocresol purple dye and heavy metals as chromium from industrial effluent by adsorption onto a modified surface of zeolite: kinetics and equilibrium study. J Environ Manag 225:120–132

Aljerf L, Choukaife AE (2015) The efficient implementation of the Jift as one of the olive mill waste (OMW) in urea extraction from urine. J King Abdulaziz Univ 26(1):101–114

Aljerf L, Nadra R (2019) Developed greener method based on MW implementation in manufacturing CNFs. Int J Nanomanufac 15(3): 269–289

Alslaibi TM, Abustan I, Ahmad MA, Foul AA (2013) Cadmium removal from aqueous solution using microwaved olive stone activated carbon. J Environ Chem Eng 1:589–599

Anitha T, Senthil Kumar P, Sathish Kumar K (2015) Binding of Zn(II) ions to chitosan–PVA blend in aqueous environment: adsorption kinetics and equilibrium studies. Environ Prog Sustain 34:15–22

Ardelean IL, Stoencea LBN, Ficai D et al (2017) Development of stabilized magnetite nanoparticles for medical applications. J Nanomater 6514659:9

Azari A, Gharibi H, Kakavandi B, Ghanizadeh G, Javid A, Mahvi AH, Sharafi K, Khosravia T (2017) Magnetic adsorption separation process: an alternative method of mercury extracting from aqueous solution using modified chitosan coated Fe3O4 nanocomposites. J Chem Technol Biotechnol 92:188–200

Behdani FN, Rafsanjani AT, Torab-Mostaedi M, Mohammadpour SMAK (2013) Adsorption ability of oxidized multiwalled carbon nanotubes towards aqueous Ce(III) and Sm(III). Korean J Chem Eng 30:448–455

Boushehrian MM, Esmaeili H, Foroutan R (2020) Ultrasonic assisted synthesis of kaolin/CuFe2O4 nanocomposite for removing cationic dyes from aqueous media. J Environ Chem Eng 8:103869

Chen T, Yan C, Wang Y, Tang C, Zhou S, Zhao Y, Ma R, Duan P (2015) Synthesis of activated carbon-based amino phosphonic acid chelating resin and its adsorption properties for Ce(III) removal. Environ Technol 36:2168–2176

Dada AO, Olalekan AP, Olatunya AM et al (2012) Langmuir, Freundlich, Temkin and Dubinin–Radushkevich isotherms studies of equilibrium sorption of Zn2+ unto phosphoric acid modified rice husk. IOSR J Appl Chem 3:38–45

Dorabei RZ, Jalalat V, Tadjarodi A (2016) Central composite design optimization of Ce(III) ion removal from aqueous solution using modified SBA-15 mesoporous silica. NJC 40:5128–5134

Doyurum S, Celik A (2006) Pb(II) and Cd(II) removal from aqueous solutions by olive cake. J Hazard Mater B138:22–28

Dubey SS, Rao BS (2011) Removal of cerium ions from aqueous solution by hydrous ferric oxide – A radiotracer study. J Hazard Mater 186: 1028–1032

Foo KY, Hameed BH (2010) Insights into the modeling of adsorption isotherm systems. Chem Eng J 156:2–10

Gunasundari E, Senthil Kumar P (2017) Adsorption isotherm, kinetics and thermodynamic analysis of Cu(II) ions onto the dried algal biomass (Spirulina platensis). J Ind Eng Chem 56:129–144

Haroon H, Ashfaq T, Gardazi SMH et al (2016) Equilibrium kinetic and thermodynamic studies of Cr(VI) adsorption onto a novel adsorbent of Eucalyptus camaldulensis waste: batch and column reactors. Korean J Chem Eng 33:2898–2907

Ho YS, McKay G (1999) Pseudo-second order model for sorption processes. Process Biochem 34:451–465

Hubbe MA, Azizian S, Douven S (2019) Implications of apparent pseudo-second-order adsorption kinetics onto cellulosic materials: a review. BioRes 14:7582–7626

Iconaru SL, Guégan R, Popa C et al (2016) Magnetite (Fe3O4) nanoparticles as adsorbents for As and Cu removal. Appl Clay Sci 134:128–135

Karimzadeh I, Aghazadeh M, Doroudi T et al (2017) Amino acid coated superparamagnetic iron oxide nanoparticles for biomedical applications through a novel efficient preparation method. J Clust Sci 28: 1259–1271

Kaveeshwar AR, Ponnusamy SK, Revellamec ED et al (2018) Pecan shell based activated carbon for removal of iron(II) from fracking wastewater: adsorption kinetics, isotherm and thermodynamic studies. Process Saf Environ Prot 14:107–122

Khdair A, Abu-Rumman G (2020) Sustainable environmental management and valorization options for olive mill byproducts in the Middle East and North Africa (MENA) Region. Processes 8(6): 671. https://doi.org/10.3390/pr8060671

Khorasani AC, Shojaosadati SA (2019) Magnetic pectin-Chlorella vulgaris biosorbent for the adsorption of dyes. J Environ Chem Eng 7(3):103062

Klika K, Seidlerová J, Valášková M et al (2016) Uptake of Ce(III) and Ce(IV) on montmorillonite. Appl Clay Sci 132–133:41–49

Kumar PS, Ramalingam S, Abhinaya RV et al (2011) Lead(II) adsorption onto sulphuric acid treated cashew nut shell. Sep Sci Technol 46: 2436–2449

Kutahyalı C, Sert S, Cetinkaya B et al (2012) Biosorption of Ce(III) onto modified Pinus brutia leaf powder using central composite design. Wood Sci Technol 46:721–736

Lazarević S, Janković-Častvan I, Djokić V et al (2010) Iron- modified sepiolite for Ni2+ sorption from aqueous solution: an equilibrium, kinetic, and thermodynamic study. J Chem Eng Data 55:5681–5689

Loddo V, Yurdakal S, Parrino F (2020) Economical aspects, toxicity, and environmental fate of cerium oxide. In: Cerium Oxide (CeO_2): Synthesis, Properties and Applications, pp 359–373. https://doi.org/10.1016/B978-0-12-815661-2.00009-8

Ma J, Wang L, Wu Y, Dong X, Ma Q, Qiao C, Zhang Q, Zhang J (2014) Facile synthesis of Fe3O4 nanoparticles with a high specific surface area. Mater Trans 55:1900–1902

Mittal V (2013) Thermoset nanocomposites. In: Technology & Engineering. Wiley. https://doi.org/10.1002/9783527659647

Nemmar A, Al-Salam S, Beegam S et al (2017) The acute pulmonary and thrombotic effects of cerium oxide nanoparticles after intratracheal instillation in mice. Int J Nanomedicine 10(12):2913–2922

Pagnanelli F, Mainelli S, Vegli F et al (2003) Heavy metal removal by olive pomace: biosorbent characterisationand equilibrium modelling. Chem Eng Sci 58:4709–4717

Pearlin Kiruba U, Senthil Kumar P, Prabhakaran C et al (2014) Characteristics of thermodynamic, isotherm, kinetic, mechanism and design equations for the analysis of adsorption in Cd(II) ions-surface modified Eucalyptus seeds system. J Taiwan Inst Chem E 45:2957–2968

Pylypchuk V, Kołodyńska D, Kozioł M et al (2016) Gd-DTPA Adsorption on chitosan/magnetite nanocomposites. Nanoscale Res Lett 11:168–177

Ramos SJ, Dinali GS, Oliveira C, Martins GC, Moreira CG, Siqueira JO, Guilherme LRG (2016) Rare earth elements in the soil environment. Curr Pollut Rep 2(1):28–50

Rim KT, Koo KH, Park JS (2013) Toxicological evaluations of rare earths and their health impacts to workers: a literature review. Saf Health Work 4(1):12–26

Sadovsky D, Brenner A, Astrachan B, Asaf B, Gonen R (2016) Biosorption potential of cerium ions using Spirulina biomass. J Rare Earths 34:644–652

Sangkarak S, Phetrak A, Kittipongvises S, Kitkaew D, Phihusut D, Lohwacharin J (2020) Adsorptive performance of activated carbon reused from household drinking water filter for hexavalent chromium-contaminated water. J Environ Manag 272:111085

Saravanan A, Senthil Kumar P, Annam Renita A (2018) Hybrid synthesis of novel material through acid modification followed ultrasonication to improve adsorption capacity for zinc removal. J Clean Prod 172: 92–105

Schneider RM, Cavalin CF, Barros MASD, Tavares CRG (2007) Adsorption of chromium ions in activated carbon. Chem Eng J 132:355–362

Sert Ş, Kütahyalı C, İnan S et al (2008) Biosorption of lanthanum and cerium from aqueous solutions by Platanus orientalis leaf powder. Hydrometallurgy 90:13–18

Serunting MA, Rusnadi R, Setyorini DA, Ramadan BS (2018) An effective cerium (III) ions removal method using sodium alginate-coated magnetite (Alg-Fe3O4) nanoparticles. J Water Supply Res T 67: 754–765

Sharma M, Kalita P, Senapati KK et al (2018) Study on magnetic materials for removal of water pollutants, emerging pollutants - some strategies for the quality preservation of our environment, Sonia Soloneski and Marcelo L. Larramendy. IntechOpen. https://doi.org/10.5772/intechopen.75700

Shojaei Z, Iravani E, Moosavian MA et al (2016) Removal of cerium from aqueous solutions by amino phosphate modified nano TiO2: kinetic, and equilibrium studies. Iran J Chem Eng 13:3–21

Suboti B, Bronic J (1986) Removal of cerium(III) species from solutions using granulated zeolites. J Radioanal Nucl Chem 102:465–481

Tamjidi S, Esmaeili H, Moghadas BK (2019) Application of magnetic adsorbents for removal of heavy metals from wastewater: a review study. Mater Res Express 6:102004

Taufiq A, Saputro RE, Sunaryono et al (2017) Fabrication of magnetite nanoparticles dispersed in olive oil and their structural and magnetic investigations. IOP Conf Ser: Mater Sci Eng 202:012008

Tora L (2003) Heavy metal removal by olive pomace: biosorbent characterisation and equilibrium modelling. Chem Eng Sci 58(20): 4709–4717

Torab-Mostaedi M (2013) Biosorption of lantanum and cerium from aqueous solutions using tangerine (Citrus reticulata) peel: equilibrium, kinetic and thermodynamic studies. Chem Ind Chem Eng Q 19: 79–88

Torab-Mostaedi M, Asadollahzadeh M, Hemmati A, Khosravi A (2015) Biosorption of lanthanum and cerium from aqueous solutions by grapefruit peel: equilibrium, kinetic and thermodynamic studies. Res Chem Intermed 41:559–573

Varsihini CJS, Das D, Das N (2014) Optimization of parameters for cerium(III) biosorption onto biowaste materials of animal and plant origin using 5-level Box-Behnken design: equilibrium, kinetic, thermodynamic and regeneration studies. J Rare Earths 32:745–758

Vijayaraghavan K, Balasubramanian R (2010) Single and binary biosorption of cerium and europium onto crab shell particles. Chem Eng J 163:337–343

Vijayaraghavan K, Sathishkumar M, Balasubramanian R (2010) Biosorption of lanthanum, cerium, europium, and ytterbium by a brown marine alga, Turbinaria Conoides. Ind Eng Chem Res 49: 4405–4411

Yan Y, Sarkar B, Zhou L, Zhang L, Li Q, Yang J, Bolan N (2020) Phosphorus-rich biochar produced through bean-worm skin waste pyrolysis enhances the adsorption of aqueous lead. Environ Pollut 266:115177

Yi Y, Lv J, Liu Y, Wu G (2017) Synthesis and application of modified Litchi peel for removal of hexavalent chromium from aqueous solutions. J Mol Liq 225:28–33

Yusan S, Korzhynbayeva K, Aytas S, Tazhibayeva S, Musabekov K (2014) Preparation and investigation of structural properties of magnetic diatomite nanocomposites formed with different iron content. J Alloys Compd 608:8–13